Fermi Surface Evolution and Luttinger Theorem in Na_xCoO_2: A Systematic Photoemission Study

H.-B. Yang,[1] Z.-H. Pan,[1] A. K. P. Sekharan,[2] T. Sato,[2] S. Souma,[2] T. Takahashi,[2] R. Jin,[3] B. C. Sales,[3] D. Mandrus,[3] A. V. Fedorov,[4] Z. Wang,[1] and H. Ding[1]

[1]*Department of Physics, Boston College, Chestnut Hill, Massachusetts 02467, USA*
[2]*Department of Physics, Tohoku University, 980-8578 Sendai, Japan*
[3]*Condensed Matter Science Division, Oak Ridge National Laboratory, Oak Ridge, Tennessee 37831, USA*
[4]*Advanced Light Source, Lawrence Berkeley National Laboratory, Berkeley, California 94720, USA*

(Received 17 January 2005; published 27 September 2005)

We report a systematic angle-resolved photoemission study on Na_xCoO_2 for a wide range of Na concentrations ($0.3 \leq x \leq 0.72$). In all the metallic samples at different x, we observed (i) only a single holelike Fermi surface centered around Γ and (ii) its area changes with x according to the Luttinger theorem. We also observed a surface state that exhibits a larger Fermi surface area. The e_g' band and the associated small Fermi surface pockets near the K points predicted by band calculations are found to sink below the Fermi energy in a manner almost independent of the doping and temperature.

DOI: 10.1103/PhysRevLett.95.146401 PACS numbers: 71.27.+a, 71.18.+y, 74.25.Jb, 74.70.−b

The surprising discovery of superconductivity on $Na_xCoO_2 \cdot yH_2O$ [1] raises many questions on the nature of pairing and its connection to the high-T_c superconductivity. The phase diagram of the cobaltate $Na_xCoO_2 \cdot yH_2O$, with varying electron doping x and water intercalation y over a wide range, is very rich and complicated. In addition to superconductivity, it exhibits charge order, magnetic order including a metamagnetic transition, and other structural transitions [2–5]. The physics of these phases and the transitions among them is of importance by itself, and offers an excellent platform for studying correlated triangular lattice fermion systems.

Understanding the evolution of the low-energy electronic structure such as the quasiparticle (QP) dispersion and the Fermi surface (FS) topology is a necessary step toward understanding the diverse physical properties and the nature of the pairing interaction in this class of transition metal oxide. It is therefore important to gain the precise knowledge of the FS structure and the low-energy excitations in the unhydrated Na_xCoO_2 which have been the focus in many recent theoretical and experimental efforts. The cobaltate is a multiorbital system where the Co^{4+} is in the $3d^5$ configuration, occupying the lower t_{2g} band complex similar to the ruthenate Sr_2RuO_4. First principle band calculations have predicted that Na_xCoO_2 has a large FS associated with the a_{1g} band centered around the Γ point and six small FS pockets of mostly e_g' character near the K points for a wide range of x [6,7]. Based on this band structure, it has been proposed that the large density of states contribution from the six FS pockets and the nesting condition among them enhance the spin fluctuations and lead to superconducting pairing of the QPs [8]. However, angle-resolved photoelectron spectroscopy (ARPES) measurements on the cobaltate with high Na concentrations ($x \sim 0.6$–0.7) revealed only the large FS [9,10]. It was also noticed that the enclosed FS area, i.e., the density of holes, may not satisfy the Luttinger theorem which is a fundamental QP counting rule in interacting electron systems. It is therefore desirable to study the evolution of the QP band dispersion and the FS, especially the fate of the FS pockets as a function of the Na concentration x. This is the focus of this work. We choose a set of metallic Na_xCoO_2 with $0.3 \leq x \leq 0.72$. The insulating phase at $x = 0.5$ due to Na dopant order and the magnetic phase at $x \geq 0.75$ are outside the scope of this study.

High quality single crystal Na_xCoO_2 samples were prepared by the flux method and subsequent sodium deintercalation. ARPES experiments were performed at the Synchrotron Radiation Center, WI, and the Advanced Light Source, CA. High-resolution undulator beam lines and Scienta analyzers with a capability of multiangle detection have been used. Most spectra were measured using 100 eV photons which we found to suit well for the FS mapping of Co $3d$ orbitals. However, some spectral features are better revealed at lower photon energies which will be discussed below. The energy resolution is ~10–40 meV, and the momentum resolution ~0.02 $Å^{-1}$. Samples are cleaved and measured *in situ* in a vacuum better than 8×10^{-11} Torr at low temperatures (20–40 K) on a flat (001) surface.

Because of the surface-sensitive nature of ARPES, extra care needs to be taken in assessing how much ARPES data represent the bulk electronic structure. In many cases, surface states arise from surface reconstruction. One useful way to distinguish the surface state from the bulk state is to utilize the property that the surface state is more sensitive to surface disorder. The technique used in the ARPES community is to thermally cycle a sample and thus introduce disorder to the surface. This method is often found to be very effective in removing the surface state in Sr_2RuO_4 [11,12]. On a freshly cleaved Na_xCoO_2 surface, we sometimes observed an unusual double-band dispersion [10], as shown in Fig. 1(a). However, after the thermal cycle (40 K–200 K–40 K), one of the two bands (labeled as "S" in Fig. 1) disappears, which should be regarded as a surface state. We note that this surface state has a larger Fermi vector (k_F) and a smaller Fermi velocity (v_F). The

"surviving" band (labeled as "B") is likely bulk representative. The ARPES data presented below are obtained from freshly cleaved sample surfaces, which do not show any significant surface band. We found that the band dispersion and Fermi surface in these samples are consistent with the bulk band discussed above, only with better intensity and sharper linewidth. The bulk nature of the ARPES data reported here is further verified by our x-ray ARPES which has a much longer escape length for photoelectrons. The reason we use lower photon energy here is that it has much better resolutions in both energy and momentum, which enable us to study the FS and low-energy excitations more precisely.

We start with a survey of the valence bands and its doping dependence, as shown in Fig. 2. Figures 2(a) and 2(b) show the second derivative intensity (SDI) plots (a common practice to display dispersion for broad peaks) along Γ-M for $x = 0.48$ and 0.72, respectively. There are four major band branches, with the one at $\sim$0.5 eV being assigned to the Co $3d$ t_{2g} orbitals, and the other three at $\sim$3, 4.5, 6 eV to the O $2p$ orbitals, according to local density approximation (LDA) calculation [6]. The comparison between the two doping levels, plotted in Fig. 2(c), shows a clear and nontrivial doping dependence on the energy level of these bands. For the Co $3d$ orbitals, the average energy difference between the two doping levels is $\sim$0.1 eV. However, for the O $2p$ orbitals, the energy shifts ($\sim$0.5 eV) between the two doping levels are larger. We note that this doping dependence of the O-$2p$ orbitals can explain well the doping-dependent shift of the α peak in optical conductivity measurement which is associated with the transition from the fully occupied O-p states to the unoccupied Co e_g states [13].

Zooming in on the Co-$3d$ orbitals, one can identify more dispersive features. Figures 2(d) and 2(e) display the SDI plots of $Na_{0.35}CoO_2$ on a smaller energy scale ($\sim$1.5 eV) along Γ-M and Γ-K directions, respectively. By comparing to the LDA band structure for the same Na content [7], one can assign orbital characters to the dispersive features. However, the measured occupied bandwidths ($\sim$0.7–0.8 eV) are, remarkably, narrower than the calculated ones (1.3–1.4 eV), resulting in approximately a factor of 2 in the overall bandwidth reduction, indicating the importance of strong electron correlations in this material. Note that the flat features at the unoccupied wave vectors (k) visible in Figs. 2(d) and 2(e) near the Fermi energy (E_F) may be due to the incoherent background often observed in correlated materials.

To study the low-energy excitations and the FS more closely, we further zoom in near E_F (within 0.2 eV), as shown in Fig. 3 where a sample of $Na_{0.48}CoO_2$ is measured. This time we directly display the intensity plots since the near-E_F features are much sharper [see the energy distribution curves (EDCs) in Fig. 3(a)], and the SDI plot cannot reveal the near-E_F band well due to the interference of the Fermi-Dirac function. During the ARPES measurement, we took many parallel cuts [five of them are shown in Figs. 3(b)–3(f)] in k space. It is important to have such long cuts that cover several Brillouin zones (BZs) in order to accurately determine the FS, since they can help eliminate many potential problems such as sample misalignment and matrix element effects. Indeed, we have a small misalignment of about 3° in this sample as can be seen in Fig. 3(g). Note that the intensity is much weaker in the second BZ due to the photoemission matrix element effect. The FS is determined by plotting the ARPES intensity within a narrow energy window ($\pm$2 meV) at E_F in the two-dimensional (2D) k space as shown in Fig. 3(g) where

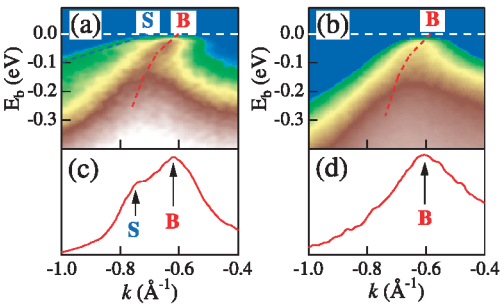

FIG. 1 (color). ARPES E-k intensity plots at $T = 40$ K on (a) a fresh surface of $Na_{0.72}CoO_2$ and (b) an aged surface of the same sample after a thermal cycle to 200 K. Red dashed lines are guides for the bulk band (marked as B), and the blue dashed line in (a) traces the surface state (marked as S). The lower panel shows the momentum distribution curves at E_F obtained on (c) the fresh surface and (d) the aged surface where the surface state vanishes.

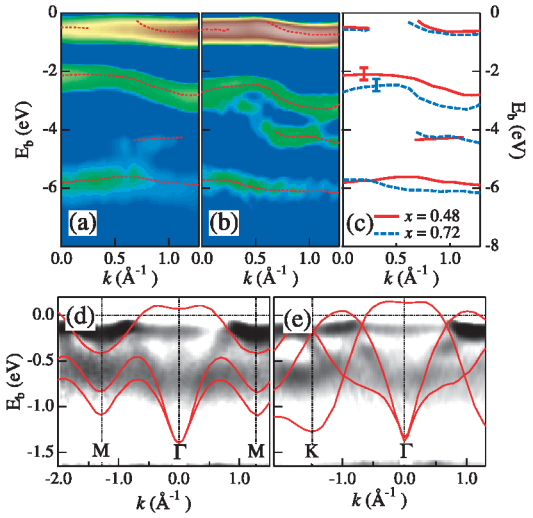

FIG. 2 (color). SDI plots of the valence bands along Γ-M for (a) $x = 0.48$ and (b) $x = 0.72$. Red dashed lines are the guides for band dispersion. (c) Comparison of Co-$3d$ and O-$2p$ orbitals between $x = 0.48$ and $x = 0.72$. The lower panel shows the SDI plots for the Co-$3d$ orbitals in $Na_{0.35}CoO_2$ along (d) Γ-M and (e) Γ-K. Red lines are band dispersions from the LDA calculation [7]. Note that the experimental uncertainty of band position is estimated to be $\pm$0.2 eV.

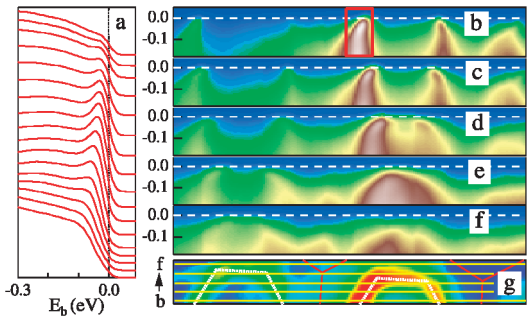

FIG. 3 (color). An example of the FS mapping on $Na_{0.48}CoO_2$. (a) Representative EDCs within the red box in panel (b). (b)–(f) E-k intensity plots along the long cuts indicated by the yellow solid lines in panel (g) where FS contours obtained from the intensity at E_F, and BZ boundaries (thin red hexagons), are plotted. White dashed lines are the guides for the FSs.

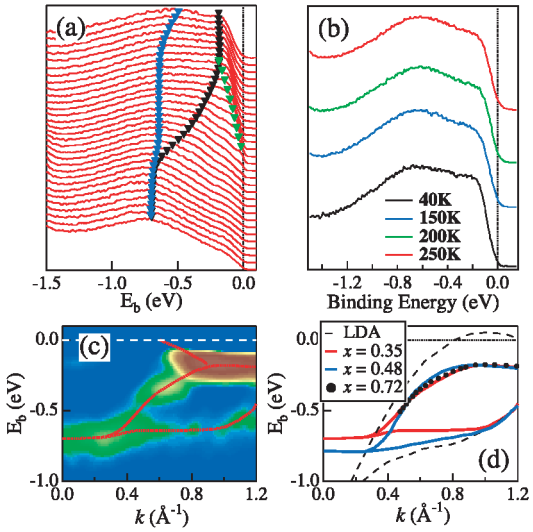

FIG. 4 (color). Sinking pockets near the K points. (a) EDCs of $Na_{0.3}CoO_2$ along Γ-K measured using 30 eV photons. Triangular markers are the guides for the band dispersion. (b) Temperature dependence of the EDC at the top of sinking pockets. (c) SDI plot for the same measurement. Red dashed lines, representing the triangular markers in panel (a), are the guides for the dispersion. (d) A comparison of the measured e_g' bands at $x = 0.3$ (red solid lines), 0.48 (blue solid lines), and 0.72 (black dots), to the LDA calculation [7] (black dashed lines).

partial FS contours over two BZs are extracted from the five long cuts shown above. We also note that the low-energy band is further renormalized due to a strong "kink" in the dispersion observed at the energy scale of 70–100 meV [see Figs. 3(b)–3(d)]. The behavior of this kink and the relationship to the well-known kink in the dispersion observed in high-T_c cuprates [14–17] will be discussed in a separate publication.

The FS we observed, as shown in Fig. 3(g), corresponds to the large a_{1g} FS centered at Γ predicted by the LDA calculation [6]. However, the six small FS pockets associated with the e_g' band predicted by the LDA are not present in our measurements for the entire range of $0.3 \leq x \leq 0.72$. Instead, we observed a broad peak that approaches but never reaches E_F near the K points, as indicated by the black triangles in Fig. 4(a). In addition, we observed two more dispersive features. The one indicated by the green triangles belongs to the a_{1g} band, and the other indicated by the blue triangles is assigned to the other e_g' band. The reason that the intensity of the a_{1g} band is much weaker in Fig. 4 than in Fig. 3 is that different photon energies were used in the two measurements. While we used 100 eV photons in Fig. 3 to enhance the Co-3d character, we found that the e_g' band near the K points is greatly enhanced at lower photon energies (30 eV in Fig. 4). This suggests a stronger mixing of O-2p character in the e_g' bands since the O p orbitals are more sensitive to the low-energy photons [10,18].

The broad e_g' bands can be observed more clearly in the SDI plot, as shown in Fig. 4(c). In comparison, the measured dispersions are reminiscent of the e_g' bands calculated by the LDA [6,7], as shown in Fig. 4(d). However, important differences exist: (1) the measured bandwidth is narrower than the calculated one; (2) the upper branch of e_g' bands does not cross the Fermi level—the predicted FS pockets "sink" below E_F. More significantly, this "sinking" pocket does *not* have doping dependence for its band top, as shown in Fig. 4(d), while the band bottom shifts with doping ($\sim$100 meV shift between $x = 0.3$ and $x = 0.48$). This behavior reminds us of the leading-edge property associated with the opening of an energy gap at the FS. However, we did not observe any clear change of the leading-edge shift ($\sim$100 meV) for temperatures up to 250 K, as shown in Fig. 4(b).

We summarize our ARPES results on the FS evolution in Na_xCoO_2 in Fig. 5. We have measured many samples and obtained well-reproducible results over a wide range of Na concentrations. Figures 5(a)–5(c) show three examples of the measured FS for $x = 0.3$, 0.48, and 0.72. Clearly, a single hexagonal holelike FS, centered at the Γ point, shrinks its size as x increases. A direct comparison of the FS contours at the four doping levels, shown in Fig. 5(d), provides more quantitative information on the FS evolution. All Fermi surfaces have a good hexagonal shape with parallel FS edges that can be connected by a nesting vector ($\vec{Q}_n$). The magnitude of $\vec{Q}_n$ is estimated to be $\sim$1.41, 1.40, 1.20, 1.18 Å^{-1} ($\pm$0.1 Å^{-1}) for $x = 0.3, 0.48, 0.6, 0.72$. Interestingly, these values are close to the reciprocal lattice vectors ΓK (1.47 Å^{-1}) and ΓM (1.28 Å^{-1}). In particular, the FS at $x = 0.3$ is observed to almost coincide with the reconstructed BZ of $\sqrt{3}$ by $\sqrt{3}$ charge ordering, suggesting possible strong charge fluctuations at this Na concentration. Interestingly, the latter was proposed as a driving force for superconductivity in the hydrated material [19]. From Fig. 5(d), we derive the carrier density from the FS area which we call the "effective Na concentration" $x' = 1–2A_{FS}/A_{BZ}$, where A_{FS} is the area enclosed by the 2D FS,

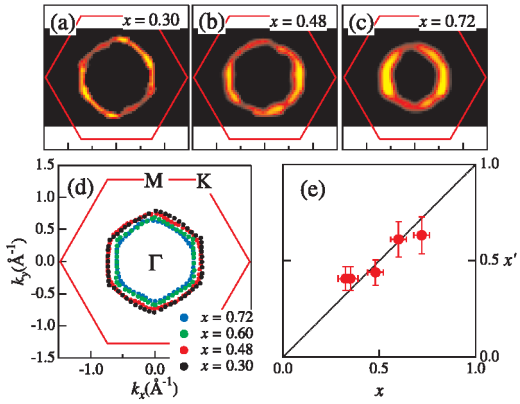

FIG. 5 (color). FS evolution in Na_xCoO_2. (a)–(c) FSs (the intensity contours at E_F) for $x = 0.3$, 0.48, and 0.72 in the first BZ (red solid lines). (d) Overlap of the FS locations at four doping levels in the BZ. (e) Effective Na concentration x' derived from FS area vs Na concentration x. The diagonal line is from the Luttinger theorem.

and A_{BZ} is the area of the BZ. In Fig. 5(e), x' is plotted versus the nominal Na concentration x. If the Luttinger theorem is satisfied, one has $x' = x$, which is indicated by the solid line in Fig. 5(e). Within the experimental uncertainties, Fig. 5(e) shows that x' tracks well the $x' = x$ line and the Luttinger theorem is thus satisfied. This helps clarify the puzzle of the FS being too large in previous ARPES results [9,10]. The conservation of the doped electron density is quite remarkable and is consistent with the nonexistence of the small FS pockets. In contrast, the FS pockets near the K points predicted by LDA calculations contribute to a significant portion of the total FS area at low doping.

The observation of the sinking pockets near the K points for such a wide range of Na concentrations is very intriguing. The qualitative discrepancy with the LDA band structure points to the importance of electronic correlation effects and is a basic unresolved issue in understanding the physical properties of the cobaltates. A recent theoretical work based on the local spin density approximation (LSDA) takes into account the local Coulomb repulsion (U) using the LSDA + U approach and finds the absence of the small FS pockets [20]. However, the disappearance of the small FS pockets in the LSDA calculation is due to the formation of a half metal with spin-split bands and spin polarized FSs, resulting in a FS area twice as large which is inconsistent with our observations. The observed behavior that the top of the sinking pocket stays at the same energy while sizable energy shifts appear at the band bottom for different doping levels is unusual and seems to suggest either the opening of a gap or more intricate many-body effects. So far, the lack of the temperature dependence of the leading edge does not appear to support the gap-opening scenario. There is recent theoretical evidence that strong correlations can push the e_g' band below E_F, leading to the disappearance of the FS pockets [21]. A better understanding of the correlation effects as well as those associated with the crystal field splitting and the hybridization with the O-2p orbitals is clearly needed in order to understand these unconventional electronic properties.

In conclusion, our ARPES results on Na_xCoO_2 over a wide range of Na concentrations ($0.3 \leq x \leq 0.72$) clearly show that there is only a single hexagonal FS centered around the Γ point, with parallel edges being possibly nested. We find that the evolution of this holelike FS obeys the Luttinger theorem. The small FS pockets near the K points predicted by the LDA calculations are found to sink below E_F with a distance to the Fermi sea almost independent of doping and temperature. These findings provide clear and detailed knowledge of the evolution of the electronic structure in Na_xCoO_2 and put constraints on the theoretical description of the superconductivity in the hydrated cobaltates.

We thank P. A. Lee and D. J. Singh for valuable discussions and suggestions, and S. Gorovikov and H. Höchst for technical support in synchrotron experiments, This work is supported by NSF DMR-0353108, DOE DE-FG02-99ER45747, Petroleum Research Fund, and the MEXT of Japan. This work is based upon research conducted at the Synchrotron Radiation Center supported by NSF DMR-0084402, and at the Advanced Light Source supported by DOE DE-AC03-76SF00098. Oak Ridge National laboratory is managed by UT-Battelle, LLC, for DOE under Contract No. DE-AC05-00OR22725.

[1] K. Takada *et al.*, Nature (London) **422**, 53 (2003).
[2] M. L. Foo *et al.*, Phys. Rev. Lett. **92**, 247001 (2004).
[3] J. L. Luo *et al.*, Phys. Rev. Lett. **93**, 187203 (2004).
[4] B. C. Sales *et al.*, Phys. Rev. B **70**, 174419 (2004).
[5] Q. Huang *et al.*, Phys. Rev. B **70**, 134115 (2004).
[6] D. J. Singh, Phys. Rev. B **61**, 13397 (2000).
[7] K.-W. Lee *et al.*, Phys. Rev. B **70**, 045104 (2004).
[8] M. D. Johannes *et al.*, Phys. Rev. Lett. **93**, 097005 (2004).
[9] M. Z. Hasan *et al.*, Phys. Rev. Lett. **92**, 246402 (2004).
[10] H.-B. Yang *et al.*, Phys. Rev. Lett. **92**, 246403 (2004).
[11] A. Damascelli *et al.*, Phys. Rev. Lett. **85**, 5194 (2000).
[12] S.-C. Wang *et al.*, Phys. Rev. Lett. **92**, 137002 (2004).
[13] N. L. Wang *et al.*, Phys. Rev. Lett. **93**, 237007 (2004).
[14] T. Valla *et al.*, Science **285**, 2110 (1999).
[15] P. V. Bogdanov *et al.*, Phys. Rev. Lett. **85**, 2581 (2000).
[16] A. Kaminski *et al.*, Phys. Rev. Lett. **86**, 1070 (2001).
[17] A. Lanzara *et al.*, Nature (London) **412**, 510 (2001).
[18] J. J. Yeh and I. Lindau, At. Data Nucl. Data Tables **32**, 1 (1985).
[19] O. I. Motrunich and P. A. Lee, Phys. Rev. B **70**, 024514 (2004).
[20] Peihong Zhang *et al.*, Phys. Rev. Lett. **93**, 236402 (2004).
[21] Sen Zhou *et al.*, Phys. Rev. Lett. **94**, 206401 (2005).